Direct Synthesis and Characterization of Zr-SBA-15 Mesoporous Molecular Sieves

GUOQIANG SONG, SHOUGAO LI, LISHENG WANG, YIN MENG and FUXIANG LI[*]

Institute of Special Chemicals, Taiyuan University of Technology, Taiyuan 030024, P.R. China

*Corresponding author: Fax: +86 351 6111178; Tel: +86 351 6010550; E-mail: L63f64x@163.com

This work reports the synthesis and characterization of Zr-SBA-15 mesoporous molecular sieves *via* direct synthesis, with $Zr(NO_3)_4 \cdot 3H_2O$ as the zirconium source. The surface features, crystalline structure and textural properties are characterized by X-ray diffraction, nitrogen adsorption-desorption isotherms, transmission electron microscopy, thermogravimetry-differential thermal analysis and electron diffraction spectroscopy. The XRD patterns and TEM micrographs of the calcined samples show the characteristic diffraction peaks of the tetragonal ZrO_2 and the ordered mesostructure in frameworks. The largest Zr/Si molar ratio during Zr-SBA-15 synthesis is 2.1. Similarly, the Brunauer-Emmett-Teller (BET) area also shows a decreasing tendency, which agrees with the XRD patterns. When the Zr/Si ratio was over 1.5, the characteristic peaks of the tetragonal ZrO_2 phase can be observed. However, when the Zr/Si ratio is 1.5 or less, the samples have a high surface area (*i.e.*, greater than 398 m^2/g), with pore diameters of approximately 7.40 nm, which are within the limits for mesoporous materials.

Keywords: Zr-SBA-15, Direct synthesis, Characterization, Mesoporous, Molecular sieves.

INTRODUCTION

Zeolites are crystalline microporous aluminosilicates with periodic arrangements of cages and channels that find extensive industrial use as catalysts, adsorbents and ion exchangers. The main advantages of ordered mesoporous materials in catalysis are their relatively larger pores compared with microporous materials such as zeolites, enabling these materials to facilitate reactant/product diffusion, as well as their high surface area, allowing the introduction of more active sites that increase the overall reaction rates of catalytic processes. However, mesoporous materials have displayed insufficient hydrothermal stability and acidity compared with conventional zeolites.

Subsequently, a new mesoporous silica named SBA-15, with periodic 5 nm to 30 nm pores, was synthesized from a polymeric silica precursor template restructured with a triblock copolymer. This material has constant pore size distribution, high surface area, thick walls and hydrothermal stability. These features provide various opportunities in the fields of catalysis, adsorption-desorption and advanced inorganic materials. However, the catalytic activity of SBA-15 is low because of its pure silica framework. Thus, doped mesoporous molecular sieves with zirconium, chromium, vanadium, manganese, *etc.* have attracted considerable attention for obtaining acid catalytic materials.

Mesoporous materials containing zirconium have received considerable attention in heterogeneous catalysis because of their high surface areas and potential acid properties, as well as their oxidation and reduction performance. The synthesis of zirconium-containing mesoporous materials has been widely reported[1-4]. One example was reported by Wang *et al.*[1] who synthesized zirconium-containing MCM-41 using direct synthesis, with $Zr(NO_3)_4 \cdot 3H_2O$ as the zirconium source, under alkalescent hydrothermal treatment. Their results showed that the Brunauer-Emmett-Teller (BET) surface area of the as-synthesized Zr-MCM-41 decreased with increasing zirconium content and that the maximum molar ratio (Zr/Si) in their samples was 0.05. Flego *et al.*[2] described SiO_2-ZrO_2 mesoporous oxides that were successfully synthesized through the sol process. They discovered that the amount of acid active sites and the intensity of these sites were both enhanced with increasing zirconium content. Klein *et al.*[3] reported that zirconium-containing amorphous porous oxides directly synthesized by the sol process could still maintain a certain surface area even when heated up to 1000 °C. Moreover, Wang *et al.*[4] produced a surface zirconium-containing MCM-41 mesoporous material by grafting neopentyl zirconium onto the MCM-41 surface in a vacuum environment, followed by processing oxidation and hydrolysis. In their study, the conversion rate of cyclohexene in the liquid-phase catalytic oxidation reaction was improved using the as-synthesized material as the catalyst. Zirconium-

containing mesoporous materials such as MCM-41 and SBA-15 inevitably form a large zirconia crystal outside the channels when ZrO_2 loading exceeds 40 %. As a result, the surface area rapidly decreases and the catalytic activity of the materials is much lower than that of bulk SO_4^{2-}/ZrO_2[5-10]. Several attempts have succeeded in introducing zirconium into the framework of molecular sieves during synthesis. However, materials with a Zr/Si ratio lower than 0.025 were produced[11]. Garg *et al.*[12] have synthesized SBA-15 containing various amount (10-50 wt. %) of highly dispersed ZrO_2 using urea hydrolysis method. They found that BET surface area and total pore volume decreased from 696 to 325 m^2/g and 0.96 to 0.52 cm^3/g, respectively, after addition of 35 wt. % of sulfated ZrO_2 to SBA indicating that the added sulfated ZrO_2 could be mainly located inside the SBA mesoporous channels. Newalkar *et al.*[13] successfully prepared mesoporous SBA-15 molecular silica substituted with zirconium with various Si/Zr ratios at 373 K under microwave-hydrothermal conditions. Their experiment results indicated that, the Zr-SBA-15 could be crystallized without any decrease in mesopore size *via* the direct synthesis approach under microwave-hydrothermal conditions and showed that, microwave-assisted synthesis is an ideal approach to prepare Zr-substituted SBA-15, which is expected to be useful as a selective oxidation catalyst for reactions involving large molecules. Chen *et al.*[14] developed an environmentally friendly process of synthesizing Zr-incorporated mesoporous SBA-15 silica materials, where no addition of mineral acids was necessary. The main strategy of this method was to utilize the acidity self-generated in the aqueous solutions of the zirconium precursors as the catalyst for TEOS hydrolysis. They also found that the morphology of the Zr-SBA-15 material varied with the acidity of the synthesis gels.

But the reports on Zr-SBA-15 synthesis with direct synthesis method in a strong acidic environment is less and this method is a significant way to synthesize doped silica mesoporous molecular sieves. The simultaneous addition of a silica source and an inorganic heteroatom source into the synthesis mixtures, if it met favorable reaction conditions, could effectively enable the access of the inorganic heteroatom into the framework of the molecular sieves, such that doped mesoporous molecular sieves are successfully synthesized. Therefore, the direct addition of $Zr(NO_3)_4·3H_2O$ (as the Zr source) into the SBA-15 synthesis mixtures and the optimization of the conditions to synthesize zirconium-containing mesoporous molecular sieves were studied in this paper. To the greatest possible extent, this process should improve the zirconium content in the molecular sieve, such that it could help in the preparation of superacid mesoporous materials.

In this research, the higher zirconium-containing mesoporous material Zr-SBA-15 was successfully synthesized *via* direct synthesis, utilizing $Zr(NO_3)_4·3H_2O$ as the zirconium source under a hydrothermal system.

EXPERIMENTAL

Tetraethylorthosilicate (TEOS, A.R, Tianjin Kemiou Chemical Reagent Co., Ltd.) and zirconium nitrate $(Zr(NO_3)_4·3H_2O$, A.R, Nanjing Cinor Chemical Technology Co., Ltd.) were used as the silicon and zirconium sources,

respectively. EO20PO70EO20 (P123, molecular weight is 5800, Aldrich Chemical Company Inc.) was used as the templates.

Characterization: X-ray diffraction (XRD) patterns were recorded with a Rigaku/max-2500 diffractometer equipped with CuK_α (λ = 0.15418 nm) radiation (40 kV, 100 mA) and the scan speeds were 2 °/min in low angle and 10 °/min in high angle. Nitrogen adsorption-desorption isotherms were measured at liquid nitrogen temperature (77 K) using a Quantachrome Nova 2000 e Surface Area & Pore Size Analyzer. The samples were degassed under vacuum for 3 h at 300 °C before adsorption measurements. The Brunauer-Emmett-Teller (BET) surface areas were calculated from the adsorption branch of the isotherms in the relative pressure range from 0.05 to 0.3. Pore size distribution was calculated by the Barrett-Joyner-Halenda (BJH) method using the adsorption branch. Transmission electron microscopy (TEM) and electron diffraction spectroscopy (EDS) experiments were performed on a JEM-2010 microscope with an acceleration voltage of 200 kV. For the TEM investigation, the sample was dispersed in alcohol by ultrasonic and the resultant suspension was then dropped on a carbon-coated copper grid. Thermogravimetry-differential thermal analysis (TG-DTA) was recorded with a WCT-2 microcomputer differential thermal analyzer in air and the heating rate was 15°C/min. The value of the analytical ZrO_2 (wt %) in Table-2 was calculated with a Atom Scan 16 inductively coupled plasma (ICP) atomic emission spectrometer made in Thermo Electron Corporation.

Synthesis of Zr-SBA-15: Zr-SBA-15 mesoporous molecular sieves were prepared as follows: First, 1 g of the triblock copolymer P123 was dissolved in 40 mL HCl solution (2 mol/L). After stirring for 3 h in a 40 °C water bath, 2.3 mL of tetraethylorthosilicate was fully mixed into the solution. After stirring for 2 h, a known amount of $Zr(NO_3)_4·3H_2O$ (ranging from 1.18 g to 9.24 g) was added to the reaction mixture. After stirring for 5 h, the mixture was transferred to a Teflon-lined reaction tank for further crystallization at 100 °C for 48 h. After washing with distilled water, the product was collected with filtration, dried, and then calcined in air at 600 °C for 6 h. The obtained sample was designated as Zr-SBA-15.

RESULTS AND DISCUSSION

Fig. 1 shows the XRD patterns within the 2θ range of 0.7° to 5° of the Zr-SBA-15 samples. One strong and two weak characteristic peaks of SBA-15 are clearly observed in Fig. 1, suggesting that the hexagonal structure of SBA-15 has been preserved throughout the synthesis and calcination of the Zr-SBA-15 sample. The intensity of the peak near 2θ = 0.9° decreases with increasing Zr/Si molar ratio during the synthesis process, and the peaks indexed to (110) and (200) eventually disappear, indicating the gradual decrease in the long-range order of the samples. Fig. 2 also shows the XRD patterns within the 2θ range of 20° to 70° of the Zr-SBA-15 samples calcined at 600 °C. When the Zr/Si molar ratio is lower than 1.5, no characteristic peaks pertaining to the zirconium compounds can be observed. This finding demonstrates that zirconium is fully dispersed in the SBA-15 structure. When the Zr/Si molar ratio is greater than 1.5, the characteristic peaks pertaining
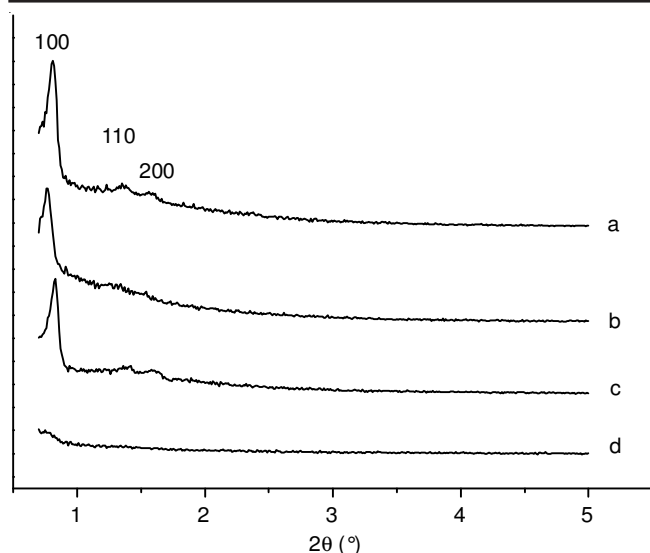
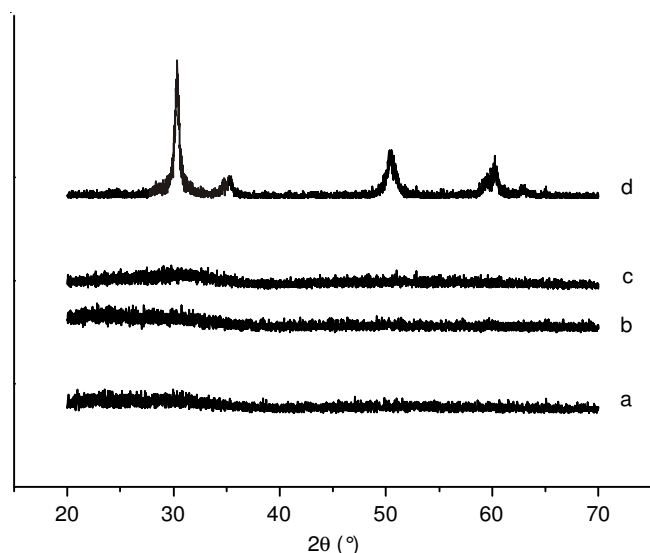Fig. 1. Low-angle XRD patterns of the Zr-SBA-15 samples Zr/Si: a-0.5, b-1.3, c-1.5, d-2.1

Fig. 2. High-angle XRD patterns of the Zr-SBA-15 samples Zr/Si: a-0.5, b-1.3, c-1.5, d-2.1

Fig. 3. N_2 adsorption-desorption isotherms Zr/Si: a-0.5, b-1.3, c-1.5, d-2.1
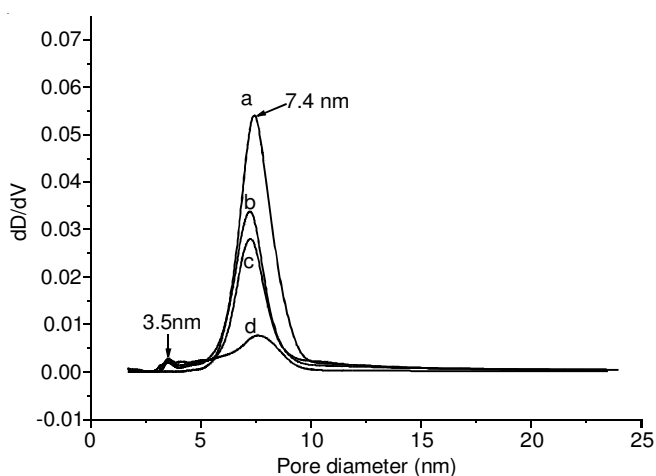
Fig. 4. Pore diameter of the Zr-SBA-15 samples. Zr/Si: a-0.5, b-1.3, c-1.5, d-2.1

TABLE-1
PORE STRUCTURE PARAMETERS OF
THE ZR-SBA-15 SAMPLES

Samples	BET area (m^2/g)	Vp (cm^3/g)	Pore diameter (nm)
Zr-SBA-15 (Zr/Si = 0.5)	546	1.13	7.44
Zr-SBA-15 (Zr/Si = 1.3)	417	0.80	7.43
Zr-SBA-15 (Zr/Si = 1.5)	398	0.73	7.44
Zr-SBA-15 (Zr/Si = 2.1)	134	0.30	7.38

to the tetragonal ZrO_2 phase can be observed, and the intensity of the peaks increases with increasing Zr/Si molar ratio. This result shows that the single particle of tetragonal ZrO_2 phase appeared in the Zr-SBA-15 samples.

The N_2 adsorption-desorption isotherms and pore size distributions of several samples are given in Figs. 3 and 4, whereas their textural properties are listed in Table-1. The isotherms of the Zr-SBA-15 samples give a clear H1 type hysteresis loop at high relative pressure, suggesting that the Zr-SBA-15 samples have very regular mesoporous channels despite their large pore size. This finding is also supported by the observed narrow Gaussian pore size distribution centered at 7.4 nm (Fig. 4). These results are very similar to those of SBA-15, implying that the mesoporous structure of SBA-15 is unchanged after the addition of Zr during synthesis, which is in agreement with the XRD results shown in Fig. 1. The BET surface area and pore volume of the Zr-SBA-15 samples decrease with increasing Zr/Si molar ratio. This result is especially true for the
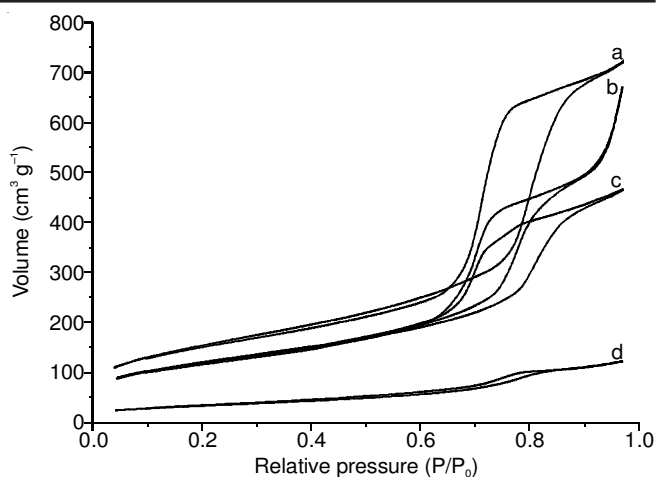
samples with Zr/Si molar ratios over 1.5, in which the pore size does not obviously change and the formation of single ZrO_2 particles outside the mesostructure chokes the pore channels at higher Zr/Si ratios, as proven by the XRD results in Fig. 2. Meanwhile, the surface area and pore volume of the Zr-SBA-15 samples are still within the ranges of 546 m^2/g to 398 m^2/g and 0.73 cm^3/g to 1.13 cm^3/g, respectively, for Zr/Si molar ratios lower than 1.5.

The calculated and analytical ZrO_2 contents in the Zr-SBA-15 mesoporous molecular sieves synthesized using different molar ratios are listed in Table-2. The corresponding virtual values are also calculated. In Table-2, the value of virtual % presents the virtual capacity of ZrO_2. And divided the value of analytical ZrO_2 (wt %) by the value of calculated ZrO_2 (wt %), we get the value of virtual %.

TABLE-2
COMPARISON BETWEEN THEORETICAL AND
EXPERIMENTAL ZrO$_2$ CONTENT

Samples	Calculated ZrO$_2$ (wt %)	Analytical ZrO$_2$ (wt %)	Virtual value (%)
Zr-SBA-15 (Zr/Si = 0.5)	50.62	16.24	32.08
Zr-SBA-15 (Zr/Si = 1.3)	72.75	24.95	34.30
Zr-SBA-15 (Zr/Si = 1.5)	75.49	28.18	37.33
Zr-SBA-15 (Zr/Si = 2.35)	82.52	80.25	97.25

The following conclusions are obtained after the comparison in Table-2. First, the concentration of ZrO$_2$ that entered the framework of SBA-15 is only approximately 30 %. The zirconium capacity of the mesoporous materials does not increase by much after reaching a Zr/Si ratio of 1.3. Furthermore, the mesoporous materials can no longer be synthesized when the Zr/Si ratio reached 2.35, that is, when the zirconium source has completely transformed into ZrO$_2$.

The TG-DTA curves with different molar ratios are shown in Fig. 5. As shown in the figure, the endothermic peaks obviously emerge in the DTA curves at 100 °C because of the desorption of the surface-adsorbed water and the crystal water.
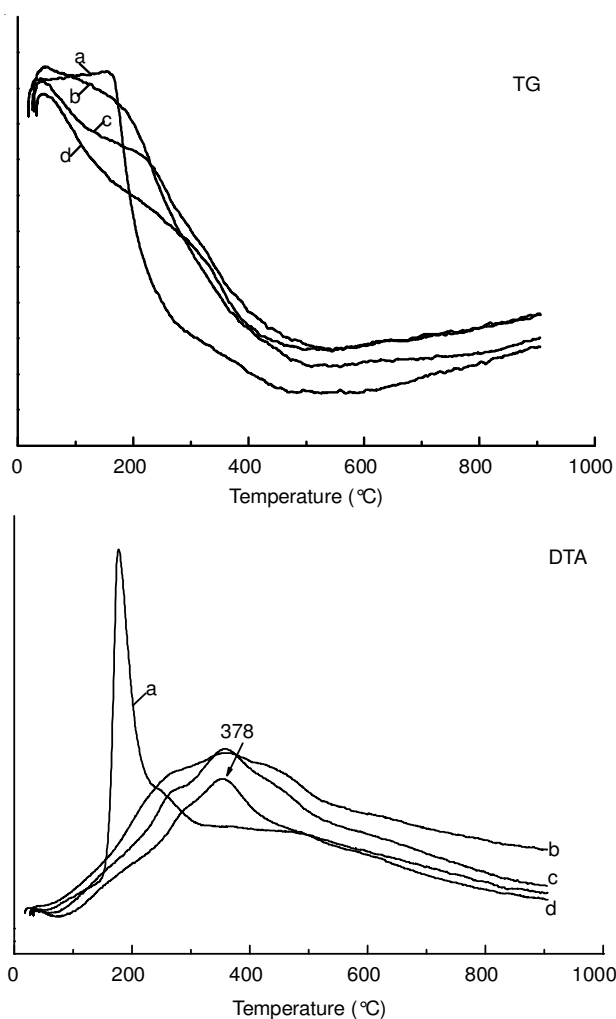
Fig. 5. TG-DTA curves of SBA-15 and different Zr-SBA-15 samples Zr/Si: a-0, b-0.5, c-1.3, d-1.5

Accordingly, the exothermic peaks that appeared at 350 °C are accompanied with weightlessness, which may have been caused by the desorption of the organic templates. However, a row of intensive exothermic peaks appear only at 190 °C in the SBA-15 curve, causing by the burning of the organic polymer template agents (P123). The TG curves suggest that the degrees of weightlessness for the samples with different molar ratios are almost equal and that all reach equilibrium at 450 °C.

The morphology of the as-synthesized Zr-SBA-15 molecular sieve powders is investigated by TEM. The TEM images of the Zr-SBA-15 samples are shown in Fig. 6. The pore diameter is approximately 7.5 nm. These results are in agreement with the N$_2$ adsorption measurements. Zirconium is obviously homogeneously dispersed onto the SBA-15 framework. As shown from the vertical direction, the ordered hexagonal structures are found to have almost no difference with those in the conventional SBA-15. These results suggest that the ordered Zr-SBA-15 material can be produced *via* direct synthesis.
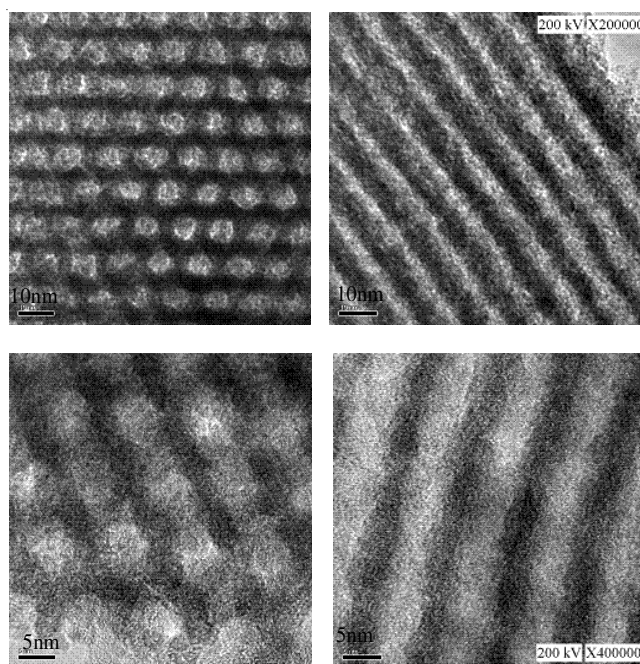
Fig. 6. TEM images of a Zr-SBA-15 sample (Zr/Si = 1.3)

The EDS spectrum for the as-synthesized Zr-SBA-15 is shown in Fig. 7. As shown in the figure, the as-synthesized sample is mainly composed of Si, Zr and O (H is not visible). This spectrum shows that the synthesized samples are composed of Si-Zr silicates.

In the synthesis system, TEOS was added to the mixture of P123 and HCl after stirring for 3 h. In order to make the completely hydrolysis of TEOS, we kept stirring the mixture for 2 h. Then, Zr(NO$_3$)$_4$·3H$_2$O was added to the reaction mixture, stirring for 5 h. We suspected that the hydrolysis rate of the TEOS and Zr(NO$_3$)$_4$ couldn't bring into perfect correspondence with the combination rate of the [(≡Si-O)$_3$Zr-O$^-$], which resulted in the low actual zirconium capacity of the samples and the ZrO$_2$ content still maintained a level of about 30 %.
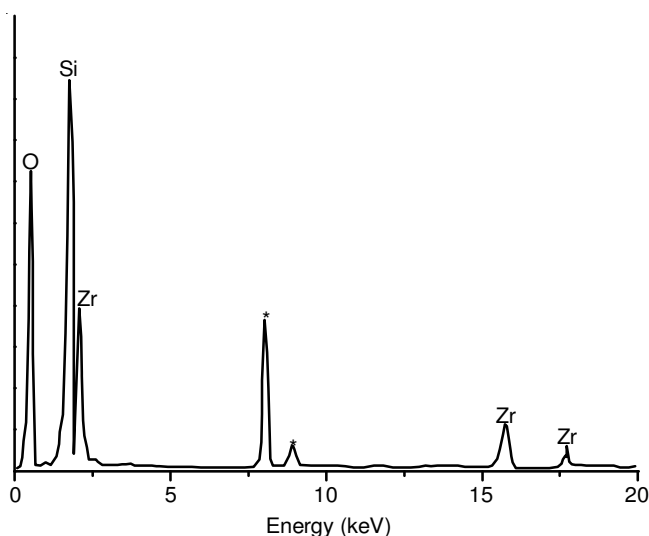
Fig. 7.   EDS spectrum of a Zr-SBA-15 sample (Zr/Si = 1.3). (*) is the Cu element from the supporting grid

Conclusion

Zr-SBA-15 mesoporous molecular sieves with high Zr/Si ratios (from 0.5 to 2.1) and a highly ordered mesostructure are synthesized *via* direct synthesis using zirconium nitrate and tetraethyl orthosilicate as the precursors, in which the Zr atoms partly connect to the framework of SBA-15 and ZrO_2 are highly dispersed. The XRD and TEM results show that the Zr-SBA-15 samples are more thermostable than bulk ZrO_2 and pure mesoporous zirconia. Based on the abovementioned analysis, the characteristic diffraction peaks of ZrO_2 not appear in the high-angle XRD patterns (Zr/Si molar ratio: 0.5-1.5) after the samples are calcined. Therefore, we speculate that $[(\equiv Si\text{-}O)_3 Zr\text{-}O^-]$ is formed because Zr^{4+} can bond with Si^{4+} and O^{2-} when $Zr(NO_3)_4 \cdot 3H_2O$ is directly added into the synthesis mixture. The final structure of the sample shows that an appropriate amount of $Zr(NO_3)_4 \cdot 3H_2O$ should be added; otherwise,

the Zr-SBA-15 mesoporous molecular sieve cannot be synthesized successfully. In addition, the results of the elemental analysis show that the actual zirconium capacity of the samples is not very high and that the ZrO_2 content still maintained a level of about 30 %, even with the increased addition of zirconium. The TEM images demonstrate that the as-synthesized Zr-SBA-15 mesoporous molecular sieves have thick pore walls that provide great support for thermostability and hydrothermal stability.

REFERENCES

1.   X.X. Wang, F. Lefebvre, J. Patarin and J. Basset, *Micropor. Mesopor. Mater*., **42**, 269 (2001).
2.   C. Flego, L. Carluccio, C. Rizzo and C. Perego, *Catal. Commun*., **2**, 43 (2001).
3.   J. Klein, C. Lettmann and W.F. Maier, *J. Non-Cryst. Solids*, **282**, 203 (2001).
4.   X.X. Wang, X. Chen and X.Z. Fu, *J. Fuel Chem. Technol.,* **29**, 4 (2001).
5.   F. Schüth, U. Ciesla, S. Schacht, M. Thieme, Q. Huo and G. Stucky, *Mater. Res. Bull*., **34**, 483 (1999).
6.   J.L. Blin, R. Flamant and B.L. Su, *Int. J. Inorg. Mater*., **3**, 959 (2001).
7.   H.R. Chen, J.L. Shi, Z.L. Hua, M.L. Ruan and D.S. Yan, *Mater. Lett.,* **51**, 187 (2001).
8.   Y. Sun, L. Zhu, H. Lu, R. Wang, S. Lin, D. Jiang and F. Xiao, *Appl. Catal. A*, **237**, 21 (2002).
9.   C.L. Chen, S. Cheng, H.P. Lin, S.T. Wong and C.Y. Mou, *Appl. Catal. A*, **215**, 21 (2001).
10.   J. He, X. Duan and C. Li, *Mater. Chem. Phys*., **71**, 221 (2001).
11.   X.X. Wang, F. Lefebvre, J. Patarin and J.M. Basset, *Micropor. Mesopor. Mater*., **42**, 269 (2001).
12.   S. Garg, K. Soni, G.M. Kumaran, R. Bal, K. Gora-Marek, J. K. Gupta, L. D. Sharma, G. M. Dhar, *Catal. Today*, **141**, 125 (2009).
13.   B.L. Newalkar, L. Olanrewaju and S.J. Komarneni, *Phys. Chem. B*, **105**, 8356 (2001).
14.   S.Y. Chen, L.Y. Jang and S. Cheng, *Chem. Mater.,* **16**, 4174 (2004).